MATERIALS SCIENCE

# Inducing superconductivity in Weyl semimetal microstructures by selective ion sputtering

Maja D. Bachmann,[1,2] Nityan Nair,[3] Felix Flicker,[3] Roni Ilan,[3,4] Tobias Meng,[5] Nirmal J. Ghimire,[6] Eric D. Bauer,[6] Filip Ronning,[6] James G. Analytis,[3,7] Philip J. W. Moll[1]*



**By introducing a superconducting gap in Weyl or Dirac semimetals, the superconducting state inherits the nontrivial topology of their electronic structure. As a result, Weyl superconductors are expected to host exotic phenomena, such as nonzero-momentum pairing due to their chiral node structure, or zero-energy Majorana modes at the surface. These are of fundamental interest to improve our understanding of correlated topological systems, and, moreover, practical applications in phase-coherent devices and quantum applications have been proposed. Proximity-induced superconductivity promises to allow these experiments on nonsuperconducting Weyl semimetals. We show a new route to reliably fabricate superconducting microstructures from the nonsuperconducting Weyl semimetal NbAs under ion irradiation. The significant difference in the surface binding energy of Nb and As leads to a natural enrichment of Nb at the surface during ion milling, forming a superconducting surface layer ($T_c$ ~ 3.5 K). Being formed from the target crystal itself, the ideal contact between the superconductor and the bulk may enable an effective gapping of the Weyl nodes in the bulk because of the proximity effect. Simple ion irradiation may thus serve as a powerful tool for the fabrication of topological quantum devices from monoarsenides, even on an industrial scale.**

## INTRODUCTION

Materials with nontrivial band structure topologies form one of the most active fields of current condensed matter research (*1*–*3*). Their unifying feature is the existence of topologically protected surface states: two-dimensional Dirac particles on the surface of topological insulators or open strings of surface states known as "Fermi arcs" in the case of three-dimensional topological semimetals. When these topological surfaces are superconducting, they may host zero-energy modes that are related to "Majorana fermions," which are proposed as one route to topological quantum computation (*4*–*6*). The key ingredient is a nonzero superconducting order parameter that breaks charge conservation on the surface, which can be achieved by either an intrinsic superconducting gap in the bulk or inducing superconductivity through coupling the surface to a superconductor. The latter opens exciting possibilities to engineer Majorana systems by combining band-inverted, strong spin-orbit–coupled topological materials with robust superconductivity, without the need to obtain both intrinsically within the same material.

In the past few years, substantial effort has been devoted to the engineering of proximity-induced topological superconductivity in the surface states of topological insulators (*7*–*22*). Because these materials are gapped in the bulk by definition, the proximity effect can only be active on their surface. A fundamentally different situation is found in topological semimetals. Here, we focus on topological Weyl semimetals (WSMs) featuring an energy gap for all momenta except a small number of topologically protected "Weyl nodes" (isolated points in the Brillouin zone at which the gap closes). WSMs require a breaking of either time-reversal or inversion symmetry. Although theoretical studies have focused mostly on the former, it is examples of the latter that have been experimentally confirmed in the monoarsenide materials (Ta,Nb)(As,P) (*23*). NbAs is one of the best-characterized WSMs, with its topological character identified by angle-resolved photoemission spectroscopy (*24*), transport (*25*, *26*), and high-field magnetization (*27*). Superconductivity in WSMs, both intrinsic and extrinsic, has been studied theoretically in recent years but has not yet been realized experimentally.

The WSM NbAs does not exhibit intrinsic superconductivity, even under high hydrostatic pressure (*28*). Methods aimed at changing the charge carrier concentration in the hope of inducing superconductivity, such as gating or chemical doping, have so far not been applied successfully without destroying the topological character of the material (*29*). A natural route to overcome this issue is to induce superconductivity via the proximity effect in NbAs. This experimental configuration is typically achieved by deposition of a superconducting thin film onto the crystalline sample (either bulk or thin film). This approach has enabled the study of proximity effect–induced superconductivity on topological insulators in two and three dimensions, as well as one-dimensional systems with strong spin-orbit coupling in geometries, such as Josephson junctions and normal-superconducting interfaces (*30*–*34*).

One outstanding obstruction on the path to a well-developed proximity-induced gap arises from the interface quality that commonly suffers from lattice mismatches and the unwanted formation of interface layers when switching between different processing materials or exposing the material to the atmosphere. Here, we present an alternative, technologically simple and effective way to reliably fabricate superconductor-WSM heterostructures. TaAs and NbAs contain elemental superconductors with sizable transition temperatures [Ta ($T_c$ = 4.5 K) and Nb ($T_c$ = 9.2 K)]. Besides the intrinsic superconductivity of these elements, their binary and tertiary compounds show a rich phase space of superconducting states with high transition temperatures, with $Nb_3Sn$ and NbTi as the most famous and commercially most important examples. This material-specific affinity to superconductivity provides the opportunity of an alternate approach to induce surface superconductivity by removing As from the surface instead of adding a superconductor onto it. If the surface of a crystal can be locally depleted of As, then an intrinsically superconducting thin film would form as a shell around the crystal.

[1]Max Planck Institute for Chemical Physics of Solids, 01187 Dresden, Germany. [2]Scottish Universities Physics Alliance, School of Physics and Astronomy, University of St. Andrews, St. Andrews KY16 9SS, U.K. [3]Department of Physics, University of California, Berkeley, Berkeley, CA 94720, USA. [4]Raymond and Beverly Sackler School of Physics and Astronomy, Tel Aviv University, Tel Aviv 69978, Israel. [5]Institut für Theoretische Physik, Technische Universität Dresden, 01062 Dresden, Germany. [6]Los Alamos National Laboratory, Los Alamos, NM 87545, USA. [7]Lawrence Berkeley National Laboratory, Berkeley, CA 94720, USA.
*Corresponding author. Email: philip.moll@cpfs.mpg.de

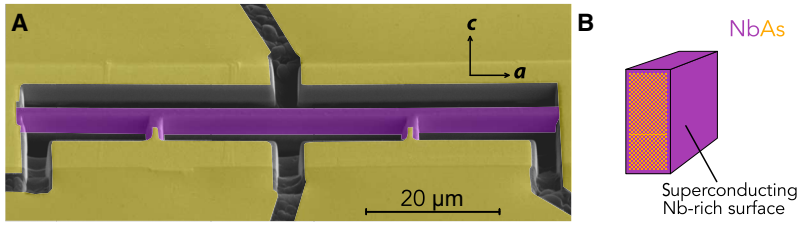


**Fig. 1. Superconducting Weyl microwires.** (**A**) Scanning electron micrograph of a typical microwire. A 100 × 20 × 3–$\mu m^3$ slice was FIB-cut from a NbAs single crystal and electrically contacted (gold leads for four-terminal measurement). The central bar (purple) was carved in a subsequent FIB etching step to ensure a homogeneous coverage of the induced superconducting layer. The bar is 2.7 μm tall and 1.8 μm wide, and the voltage contacts are 35 μm apart. (**B**) Sketch of the FIB-fabricated wire in cross section. Arsenic is preferentially sputtered from the surface, leaving a Nb-rich surface layer. The device is completely encased in the superconducting shell.

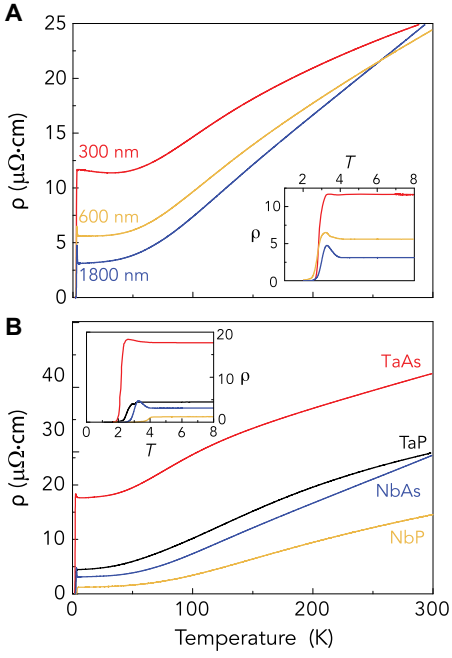


**Fig. 2. Temperature dependence of resistivity.** (**A**) Resistivity as a function of temperature for the NbAs transport bar shown in Fig. 1. The device was successively thinned down in three steps to widths of 1800, 600, and 300 nm. In this process, the height of 2700 nm did not change. The device shows a similar onset of the superconducting transition independent of the device width at 3.5 K and a zero resistance state below 2.5 K. The high-temperature resistivity is found to be strongly dependent on the device width, which reflects the presence of a second conduction channel on the surface and the resulting breakdown of ohmic scaling of the total resistance with the device cross section. (**B**) Comparison of the temperature-dependent resistivity of FIB-microstructured devices across the monoarsenide family (Ta,Nb)(As,P). Because of the self-formation of a Nb respectively Ta outer shell, all these devices exhibit superconductivity with a $T_c$ between 2 and 4 K.

## RESULTS

Low-energy ion irradiation can be used to effectively remove As from an approximately 20-nm-deep surface layer in single crystals of NbAs and induce robust type II superconductivity with a $T_c \sim 3$ K. Using a focused ion beam (FIB), selected regions of a NbAs sample can be locally irradiated, providing a simple method to form superconducting nanostructures in natural proximity to the WSM host material. This process could therefore be used to selectively turn parts of a NbAs thin-film device superconducting. Typical acceleration voltages of 30 kV for $Ga^{2+}$ are used in the FIB process (*35*), and the resulting kinetic energy of 60 keV is found to be highly effective for As depletion. During ion irradiation, the impacting ions transfer their energy to the target, and there is a probability for the target atoms to escape the solid, that is, to be sputtered. The energetics of the escape process are dominated by the surface binding energy of the constituent atoms, which can be shown to be well correlated with the heat of sublimation. Fortuitously, NbAs is a binary compound consisting of two elements with extreme sublimation points: Although As sublimates at a relatively low temperature of 887 K (34.76 kJ/mol), Nb is well known for its high boiling point of 5017 K (689.9 kJ/mol). This energetic difference already captures the essential physics of the natural self-enrichment of Nb on the surface of NbAs under ion bombardment. To further quantify this intuition, we calculated the sputter yield ratios using the SRIM-2008 (*36*) Monte Carlo–based code simulating the Ga ion impact interactions at the complete damage cascade level. At normal incidence for 60-keV Ga ions, the sputter yield is 1.70 per incident ion for Nb and 10.01 for As. Therefore, one expects a highly Nb-rich amorphous surface with a composition of $Nb_{5.88}As$ to form under sputtering equilibrium conditions, as suggested by the difference in the heat of sublimation.

Figure 1A shows a typical NbAs microstructure fabricated by FIB micromachining to study the irradiation-induced surface superconductivity. The final device is a crystal microbar with electric contacts in a four-terminal resistance configuration. During fabrication, the bar is equally irradiated from all sides to ensure that it is completely encased in a shell of ion beam–irradiated material, as shown in the sketch in Fig. 1B. The detailed fabrication recipe is provided in Materials and Methods. Typical cool-down curves for crystal bars of different cross sections are shown in Fig. 2A. The weak metallic temperature dependence is typical for semimetals. The absolute resistance of the devices cannot be explained using a simple geometric factor and a constant specific resistivity. This failure of ohmic scaling directly evidences the presence of the conductive surface layer and its role in the charge transport. More than 10 microstructures of different dimensions were fabricated, and zero-resistance superconductivity with a well-reproducible $T_c \sim 3$ K was observed in all of them. The method of ion surface treatment is equally effective in all members of the (Ta,Nb)(As,P) monoarsenide family, given the large chemical and physical similarities of (Ta,Nb) and (As,P). Accordingly, they all display superconducting transitions with $T_c \sim 2$ to 4 K (Fig. 2B). The observed $T_c$ is lower than the bulk transition temperatures of Ta and Nb, and this suppression may arise from the admixture of low-concentration (As,P) and the presence of Ga and C contamination from the FIB process at the surface. However, the presence of Ga and C in FIB-processed structures alone can be excluded as the origin of the superconductivity because similar topological semimetals, such as $Cd_3As_2$, show no signatures of superconductivity (*37*).

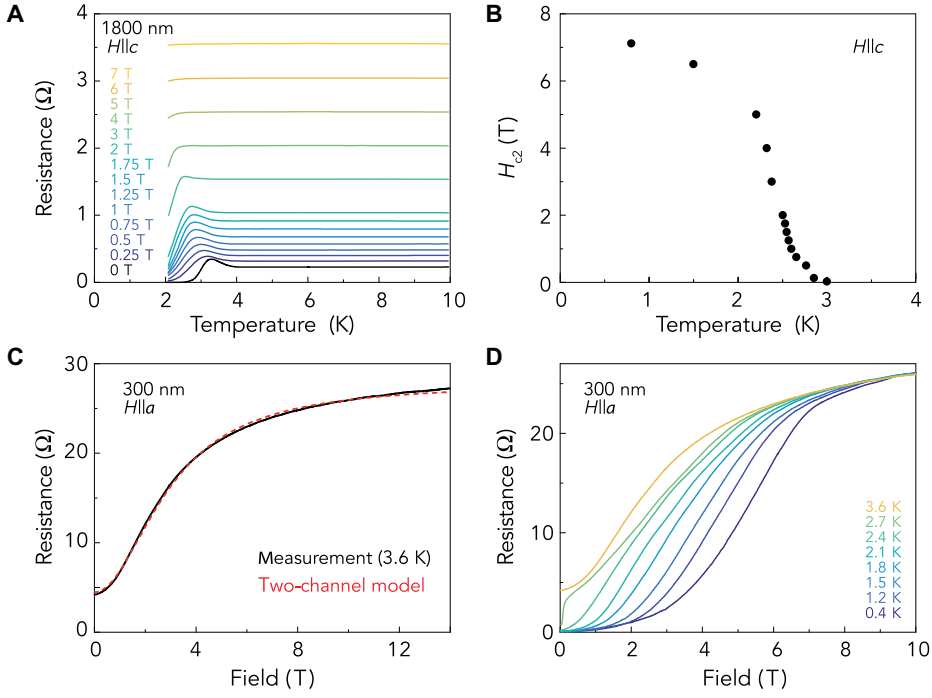


**Fig. 3. Robust superconductivity of irradiated NbAs in magnetic fields.** (**A**) Temperature dependence of the resistivity in magnetic fields applied along the crystallographic *c*-direction (1.8 × 2.7–μm cross section). The resistance peak above $T_c$ shrinks and moves to lower temperatures because superconductivity is suppressed under increasing magnetic fields. However, even in fields of 7 T, a clear sign of the transition is visible above 2 K. (**B**) Upper critical field estimated at the onset of conductivity enhancement through the superconducting transition. To avoid artifacts from the nonmonotonic temperature dependence, the upper critical field $H_{c2}(T)$ was defined at 95% of the normal state resistance, that is, $\rho(T,H_{c2}(T)) = 0.95\ \rho_n(6\text{ K},H_{c2}(T))$. Data above 2 K were determined in the 1.8-μm-wide sample, whereas the data points below 2 K were obtained in a $^3$He cryostat on the 300-nm-wide device. (**C**) Resistance of a 300-nm-wide NbAs microwire for fields applied perpendicular to the wire along the *a*-direction in the normal state. The field dependence of the device resistance can be well explained by a two-conductor model, further supporting the presence of a Nb thin film on the device surface. (**D**) Field dependence for $H||a$ at various temperatures below $T_c$. Even at temperatures close to $T_c$, large fields are required to completely suppress superconductivity and reach the two-conductor shape of the resistance.

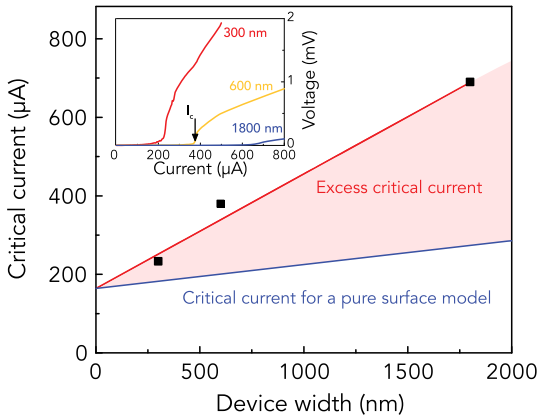


**Fig. 4. Critical currents.** Comparison of the measured width dependence of the critical current with a model based on superconductivity confined to the surface. The critical current grows stronger with increasing width than expected from a pure surface model, suggesting that the NbAs bulk plays a role in carrying supercurrents. Inset: Current-voltage characteristic of NbAs crystal bars at different widths stated in the figure but an identical thickness of 2.7 μm. For all devices, a sharp increase in voltage signals the destruction of the superconducting state at the critical current $I_c$.

## DISCUSSION

A key aspect of proximity effect–induced superconductivity concerns the quality of the interface between the superconductor and the metal. Traditionally, these heterostructures are fabricated by deposition of a superconducting metal on a nontrivial material and thus often suffer from nonideal interfaces due to surface contamination. Therefore, these structures are commonly described by a diffusive coupling of the superconductor into the metal in the dirty limit, where the range of superconductivity in the metal is limited by the short mean free path between defects, as described by the Usadel equations (*38*). The process described here leads to a self-formation of the superconductor–normal-metal interface well within the crystalline target material, which potentially enhances the transparency of the interface and thus extends the range of the proximity coupling—key to the fabrication of microstructures with a fully developed gap in the bulk.

The resistance of the microwires is temperature-independent below 10 K, and the large upper critical fields suggest a robust type II superconducting state (Fig. 3). The field dependence in the normal state provides further insight into the microscopic details of the current flow in the structures. NbAs shows a strong linear magnetoresistance for fields aligned with the crystallographic *c*-direction, which is observed above $T_c$ in the microstructures (Fig. 3A). Similar to the related compound NbP, the magnetoresistance is strongly angle-dependent, and for fields along the *a*-direction, a more conventional quadratic magnetoresistance is

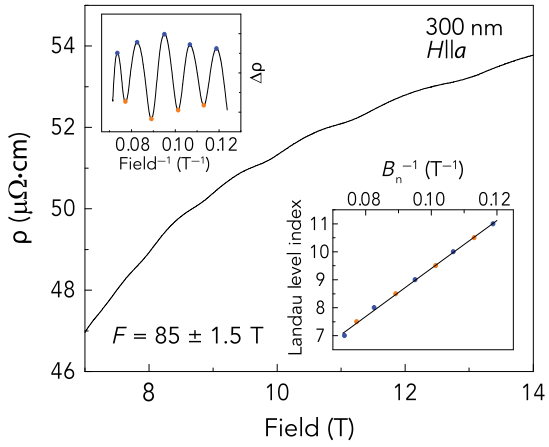


**Fig. 5. Quantum oscillations indicate bulk fermiology of NbAs.** Magnetoresistance of a 300-nm-wide device at 2 K in the normal state for fields along the crystallographic *a*-direction. Clear quantum oscillations appear on top of the magnetoresistance, even on the thinnest and hence, potentially most damaged, device. Upper inset: Same data after background subtraction, highlighting the periodic modulation of the resistivity in inverse field. Lower inset: Minima (orange) and maxima (blue) of the resistivity against the Landau level index. The straight line indicates the periodicity in inverse field, and the slope is given by the Fermi surface cross section of 85(±1.5) T.

observed (*39*). To simplify a quantitative analysis of the magnetoresistance, we focus on this $H||a$ configuration in the following discussion. In the microstructures, this quasi-quadratic magnetoresistance at low fields is followed by a successive saturation to a slower increase. This behavior can be well understood by the simple assumption of two conductive pathways in the sample, one through the pristine NbAs bulk and one through the Nb-rich layer on the surface, as depicted in Fig. 1. Assuming a usual magnetoconductivity $\sigma_{NbAs} = (a\,H^2 + \text{const.})^{-1}$ for the NbAs metal and a field-independent conductivity for the disordered Nb layer, $\sigma_{Nb}$, we arrive at a simple expression for the magnetoconductivity $\sigma = \sigma_{NbAs} + \sigma_{Nb}$, which describes the experimental field dependence (Fig. 3C) well. The fit to the data yields a resistance of the surface Nb film of 27.8 ohms for this 300-nm-wide, 2.7-μm-tall, and 10-μm-long FIB structure. This resistance of the Nb layer agrees quantitatively with measurements of FIB-irradiated Nb thin films (*40*). The fact that a simple model that assumes only two conduction channels explains the data well is further evidence for the presence of a well-defined Nb layer on the surface, instead of a gradual increase in the Nb concentration over an extended surface region.

The extent to which the superconducting region reaches into the topological semimetal via the proximity effect is an important aspect to fabricate topological microdevices. Figure 4 shows the current-voltage characteristics of a NbAs microwire at different widths. These data are taken on the same microwire, which was successively thinned down by FIB milling after each *I*-*V* measurement, to exclude any device-dependent issues. A well-defined critical current is observed at each step width, and a clear trend of the critical current is shown in the inset in Fig. 4. The critical current depends approximately linearly on the device width. For a homogeneous bulk superconductor thinner than the magnetic penetration length, the critical current is expected to scale with the device width, that is, $I_c(w) = j_c(wh)$, where $h$ denotes the constant height of the sample during thinning and $w$ is the lateral width varied by the thinning experiments. Trivially, a zero critical current arises at zero width in this case, which appears to be at odds with the present data, suggesting a finite intercept. However, a finite intercept would be natural for superconductivity in a thin surface layer around a metal. Ignoring a potential contribution of proximity effect–induced superconductivity in the bulk, an infinitesimally thin superconducting surface layer may be assumed, leading to a trivial scaling of the critical current in the heterostructure: Because all currents flow exclusively on the surface, the critical current density should be proportional to the circumference, $I_c(w) = \alpha\,(2h + 2w)$, where α is a parameter describing the critical current per unit length of the surface film. At zero width of the metallic core, a finite critical current, $I_c\,(0) = 2\alpha h$, is expected because of the currents carried by the infinitesimally thin sidewalls.

The width scaling thus supports a superconducting shell scenario, yet at the same time is consistent with supercurrents in an extended proximity effect–induced layer of finite thickness in the semimetallic bulk. The fabrication conditions for top wall and sidewalls are identical in terms of ion current density, acceleration voltage, and grazing incidence angle. Thus, it is natural to assume that the critical current parameter α does not change between top and side surfaces. Using the experimentally estimated intercept, $I_c(0)$ = 164 μA, and the measured device height, $h$ = 2.7 μm, the only free parameter in this scenario can be estimated as α = 30.4 μA/μm. This model of supercurrents confined to the thin film on the surface, $I_c(w)$ = 60.7 μA/μm $(h + w)$ matches the experimental intercept by design, but it underestimates the experimentally observed slope (blue line). This suggests that the critical current grows faster than the circumference of the device, which would be a natural consequence of supercurrents flowing in an extended region in the microwire bulk. The next step toward confirming topological superconductivity in these structures will be to integrate the superconducting microwires into phase-coherent heterostructures, such as Josephson junctions. These experiments probe the superconducting phase gradient in a topological superconductor directly and would provide the strongest evidence for superconductivity in the NbAs core via the appearance of a half-flux quantum in the Fraunhofer pattern.

The results presented here establish robust superconductivity in FIB-prepared microstructures of NbAs. At the same time, the irradiation with Ga ions is associated with a deterioration of the material quality and could potentially have destroyed the crystal structure of the material. The resulting amorphous bar could hence be a robust but topologically trivial superconductor. However, the experiment consistently evidences that the FIB-prepared microstructures of NbAs retain the high quality of the parent crystal beneath the 20-nm-deep Nb-rich shell. Figure 5 shows the magnetoresistance at 2 K in the normal state, showing pronounced Shubnikov–de Haas oscillations. These oscillations in the density of states arise from quantum-coherent motion of quasi-particles around the Fermi surface and thus are well known to be exponentially suppressed even at small defect densities (*41*). Their observation is a clear indication that the crystalline symmetry is preserved in the devices. At the same time, the appearance of a single frequency suggests that a well-defined Fermi surface at one single chemical potential exists in the core. This excludes an extended region of a chemical potential gradient and thus further evidences that the region of As deficiency is confined to a thin defect layer encasing the structure. The observed frequency of 85(±1.5) T is in agreement with previous reports of de Haas–van Alphen oscillations at 84 T obtained from bulk crystals for the given field configuration ($H||a$) (*26*, *27*). This quantitative agreement evidences the unchanged position of the chemical potential compared to bulk crystals, thereby excluding a Lifshitz transition to a topologically trivial state because of effective charge carrier doping during the irradiation process.

The fabrication of proximity effect–induced superconducting heterostructures is exceedingly demanding on the purity of the starting materials and the cleanliness of the fabrication process, because even slight contaminations of the interface between the materials form an effective barrier that strongly suppresses the Cooper pair tunneling amplitude—a well-known complication for the industrial fabrication of superconducting junctions, such as superconducting quantum interference devices (SQUIDs). Our process of ion irradiation of NbAs/TaAs thin films requires only a single material synthesis step, and the interface between the topological metal and the superconductor is formed within the material itself. Low-voltage, broadband ion irradiation, such as Ar-ion sputtering, is a standard technique in chip fabrication and can easily be combined with photolitographic or electrolithographic techniques to selectively turn parts of a circuit superconducting. We thus envision this process to be a promising route to fabricate topological superconductor heterostructures on a large scale.

## MATERIALS AND METHODS

### Ion beam surface treatment

All studied samples were fabricated in a FEI Helios NanoLab FIB, and an acceleration voltage of 30 kV was used. To ensure a homogeneous coating of the microwires with the Nb-enriched surface layer, we developed a sample fabrication scheme that exposed all surfaces equally to the ion irradiation. The procedure started on a large, flat growth face of a single crystal of NbAs.

First, a $120 \times 20 \times 3$–$\mu m^3$ slice was cut from a millimeter-sized single crystal of NbAs, transferred to a $Si/SiO_2$ substrate, and mounted in an epoxy droplet. Electrical contacts were fabricated by direct gold evaporation, followed by an ion-milling step to remove the gold from the main device. Second, the device was reintroduced into the FIB chamber and fine-structured into the final form shown in Fig. 1 using an intermediate current of 800 pA. Finally, the sidewalls of the structure were fine-polished to the target width using a fine current of 80 pA.

### Crystal growth

The growth of NbAs crystals used for this study has been previously reported (*25*). Single crystals of NbAs were grown by vapor transport using iodine as the transport agent. First, polycrystalline NbAs was prepared by heating stoichiometric amounts of Nb and As in an evacuated silica ampoule at 700°C for 3 days. Subsequently, the powder was loaded in a horizontal tube furnace in which the temperature of the hot zone was kept at 950°C and that of the cold zone was ≈850°C. Several NbAs crystals formed with distinct well-faceted flat plate–like morphology. The crystals of NbAs were verified by checking (00l) reflections on an x-ray diffractometer and by compositional analysis conducted using energy-dispersive x-ray spectroscopy (EDS). An atomic percentage ratio of Nb/As = 53:47 was obtained on the EDS measurements, which was close to the expected uncertainty of 3 to 5%.

## REFERENCES AND NOTES


1. X. Wan, A. M. Turner, A. Vishwanath, S. Y. Savrasov, Topological semimetal and Fermi-arc surface states in the electronic structure of pyrochlore iridates. *Phys. Rev. B* **83**, 205101 (2011).
2. X.-L. Qi, S.-C. Zhang, Topological insulators and superconductors. *Rev. Mod. Phys.* **83**, 1057–1110 (2011).
3. B. A. Bernevig, It's been a Weyl coming. *Nat. Phys.* **11**, 698–699 (2015).
4. J.-P. Xu, C. Liu, M.-X. Wang, J. Ge, Z.-L. Liu, X. Yang, Y. Chen, Y. Liu, Z.-A. Xu, C.-L. Gao, D. Qian, F.-C. Zhang, J.-F. Jia, Artificial topological superconductor by the proximity effect. *Phys. Rev. Lett.* **112**, 217001 (2014).
5. C. W. J. Beenakker, Search for Majorana fermions in superconductors. *Annu. Rev. Condens. Matter Phys.* **4**, 113–136 (2013).
6. J. Alicea, New directions in the pursuit of Majorana fermions in solid state systems. *Rep. Prog. Phys.* **75**, 076501 (2012).
7. L. Fu, C. L. Kane, Superconducting proximity effect and Majorana fermions at the surface of a topological insulator. *Phys. Rev. Lett.* **100**, 096407 (2008).
8. D. Zhang, J. Wang, A. M. DaSilva, J. S. Lee, H. R. Gutierrez, M. H. W. Chan, J. Jain, N. Samarth, Superconducting proximity effect and possible evidence for Pearl vortices in a candidate topological insulator. *Phys. Rev. B* **84**, 165120 (2011).
9. M. Veldhorst, M. Snelder, M. Hoek, T. Gang, V. K. Guduru, X. L. Wang, U. Zeitler, W. G. van der Wiel, A. A. Golubov, H. Hilgenkamp, A. Brinkman, Josephson supercurrent through a topological insulator surface state. *Nat. Mater.* **11**, 417–421 (2012).
10. F. Yang, F. Qu, J. Shen, Y. Ding, J. Chen, Z. Ji, G. Liu, J. Fan, C. Yang, L. Fu, L. Lu, Proximity-effect-induced superconducting phase in the topological insulator $Bi_2Se_3$. *Phys. Rev. B* **86**, 134504 (2012).
11. P. Zareapour, A. Hayat, S. Y. F. Zhao, M. Kreshchuk, A. Jain, D. C. Kwok, N. Lee, S.-W. Cheong, Z. Xu, A. Yang, G. D. Gu, S. Jia, R. J. Cava, K. S. Burch, Proximity-induced high-temperature superconductivity in the topological insulators $Bi_2Se_3$ and $Bi_2Te_3$. *Nat. Commun.* **3**, 1056 (2012).
12. J. R. Williams, A. J. Bestwick, P. Gallagher, S. S. Hong, Y. Cui, A. S. Bleich, J. G. Analytis, I. R. Fisher, D. Goldhaber-Gordon, Unconventional Josephson effect in hybrid superconductor-topological insulator devices. *Phys. Rev. Lett.* **109**, 056803 (2012).
13. M. Kriener, K. Segawa, Z. Ren, S. Sasaki, Y. Ando, Bulk superconducting phase with a full energy gap in the doped topological insulator $Cu_xBi_2Se_3$. *Phys. Rev. Lett.* **106**, 127004 (2011).
14. B. Sacépé, J. B. Oostinga, J. Li, A. Ubaldini, N. J. G. Couto, E. Giannini, A. F. Morpurgo, Gate-tuned normal and superconducting transport at the surface of a topological insulator. *Nat. Commun.* **2**, 575 (2011).
15. G. Koren, T. Kirzhner, E. Lahoud, K. B. Chashka, A. Kanigel, Proximity-induced superconductivity in topological $Bi_2Te_2Se$ and $Bi_2Se_3$ films: Robust zero-energy bound state possibly due to Majorana fermions. *Phys. Rev. B* **84**, 224521 (2011).
16. J. B. Oostinga, L. Maier, P. Schüffelgen, D. Knott, C. Ames, C. Brüne, G. Tkachov, H. Buhmann, L. W. Molenkamp, Josephson supercurrent through the topological surface states of strained bulk HgTe. *Phys. Rev. X* **3**, 021007 (2013).
17. I. Sochnikov, L. Maier, C. A. Watson, J. R. Kirtley, C. Gould, G. Tkachov, E. M. Hankiewicz, C. Brüne, H. Buhmann, L. W. Molenkamp, K. A. Moler, Nonsinusoidal current-phase relationship in Josephson junctions from the 3D topological insulator HgTe. *Phys. Rev. Lett.* **114**, 066801 (2015).
18. C. Kurter, A. D. K. Finck, Y. S. Hor, D. J. Van Harlingen, Evidence for an anomalous current–phase relation in topological insulator Josephson junctions. *Nat. Commun.* **6**, 7130 (2015).
19. J.-P. Xu, M.-X. Wang, Z. L. Liu, J.-F. Ge, X. Yang, C. Liu, Z. A. Xu, D. Guan, C. L. Gao, D. Qian, Y. Liu, Q.-H. Wang, F.-C. Zhang, Q.-K. Xue, J.-F. Jia, Experimental detection of a Majorana mode in the core of a magnetic vortex inside a topological insulator-superconductor $Bi_2Te_3/NbSe_2$ heterostructure. *Phys. Rev. Lett.* **114**, 017001 (2015).
20. I. Sochnikov, A. J. Bestwick, J. R. Williams, T. M. Lippman, I. R. Fisher, D. Goldhaber-Gordon, J. R. Kirtley, K. A. Moler, Direct measurement of current-phase relations in superconductor/topological insulator/superconductor junctions. *Nano Lett.* **13**, 3086–3092 (2013).
21. A. D. K. Finck, C. Kurter, Y. S. Hor, D. J. Van Harlingen, Phase coherence and Andreev reflection in topological insulator devices. *Phys. Rev. X* **4**, 041022 (2014).
22. S. Hart, H. Ren, T. Wagner, P. Leubner, M. Mühlbauer, C. Brüne, H. Buhmann, L. W. Molenkamp, A. Yacoby, Induced superconductivity in the quantum spin Hall edge. *Nat. Phys.* **10**, 638–643 (2014).
23. S.-M. Huang, S.-Y. Xu, I. Belopolski, C.-C. Lee, G. Chang, B. Wang, N. Alidoust, G. Bian, M. Neupane, C. Zhang, S. Jia, A. Bansil, H. Lin, M. Z. Hasan, A Weyl fermion semimetal with surface Fermi arcs in the transition metal monopnictide TaAs class. *Nat. Commun.* **6**, 7373 (2015).
24. S.-Y. Xu, N. Alidoust, I. Belopolski, Z. Yuan, G. Bian, T.-R. Chang, H. Zheng, V. N. Strocov, D. S. Sanchez, G. Chang, C. Zhang, D. Mou, Y. Wu, L. Huang, C.-C. Lee, S.-M. Huang, B. Wang, A. Bansil, H.-T. Jeng, T. Neupert, A. Kaminski, H. Lin, S. Jian, M. Z. Hasan, Discovery of a Weyl fermion state with Fermi arcs in niobium arsenide. *Nat. Phys.* **11**, 748–754 (2015).
25. N. J. Ghimire, Y. Luo, M. Neupane, D. J. Williams, E. D. Bauer, F. Ronning, Magnetotransport of single crystalline NbAs. *J. Phys. Condens. Matter* **27**, 152201 (2015).
26. Y. Luo, N. J. Ghimire, M. Wartenbe, H. Choi, M. Neupane, R. D. McDonald, E. D. Bauer, J. Zhu, J. D. Thompson, F. Ronning, Electron-hole compensation effect between topologically trivial electrons and nontrivial holes in NbAs. *Phys. Rev. B* **92**, 205134 (2015).

27. P. J. W. Moll, A. C. Potter, N. L. Nair, B. J. Ramshaw, K. A. Modic, S. Riggs, B. Zeng, N. J. Ghimire, E. D. Bauer, R. Kealhofer, F. Ronning, J. G. Analytis, Magnetic torque anomaly in the quantum limit of Weyl semimetals. *Nat. Commun.* **7**, 12492 (2016).
28. Y. Luo, N. J. Ghimire, E. D. Bauer, J. D. Thompson, F. Ronning, 'Hard' crystalline lattice in the Weyl semimetal NbAs. *J. Phys. Condens. Matter* **28**, 055502 (2016).
29. F. Arnold, C. Shekhar, S.-C. Wu, Y. Sun, R. D. dos Reis, N. Kumar, M. Naumann, M. O. Ajeesh, M. Schmidt, A. G. Grushin, J. H. Bardarson, M. Baenitz, D. Sokolov, H. Borrmann, M. Nicklas, C. Felser, E. Hassinger, B. Yan, Negative magnetoresistance without well-defined chirality in the Weyl semimetal TaP. *Nat. Commun.* **7**, 11615 (2016).
30. S. Nadj-Perge, I. K. Drozdov, J. Li, H. Chen, S. Jeon, J. Seo, A. H. MacDonald, B. A. Bernevig, A. Yazdani, Observation of Majorana fermions in ferromagnetic atomic chains on a superconductor. *Science* **346**, 602–607 (2014).
31. V. Mourik, K. Zuo, S. M. Frolov, S. R. Plissard, E. P. A. M. Bakkers, L. P. Kouwenhoven, Signatures of Majorana fermions in hybrid superconductor-semiconductor nanowire devices. *Science* **336**, 1003–1007 (2012).
32. A. Das, Y. Ronen, Y. Most, Y. Oreg, M. Heiblum, H. Shtrikman, Zero-bias peaks and splitting in an Al–InAs nanowire topological superconductor as a signature of Majorana fermions. *Nat. Phys.* **8**, 887–895 (2012).
33. M. T. Deng, C. L. Yu, G. Y. Huang, M. Larsson, P. Caroff, H. Q. Xu, Anomalous zero-bias conductance peak in a Nb–InSb nanowire–Nb hybrid device. *Nano Lett.* **12**, 6414–6419 (2012).
34. W. Chang, S. M. Albrecht, T. S. Jespersen, F. Kuemmeth, P. Krogstrup, J. Nygård, C. M. Marcus, Hard gap in epitaxial semiconductor–superconductor nanowires. *Nat. Nanotechnol.* **10**, 232–236 (2015).
35. L. A. Gianuzzi, F. A. Stevie, *Introduction to Focused Ion Beams* (Springer, 2005).
36. J. F. Ziegler, SRIM-2003. *Nucl. Instrum. Methods Phys. Res. B* **219–220**, 1027–1036 (2004).
37. P. J. W. Moll, N. L. Nair, T. Helm, A. C. Potter, I. Kimchi, A. Vishwanath, J. G. Analytis, Transport evidence for Fermi-arc-mediated chirality transfer in the Dirac semimetal $Cd_3As_2$. *Nature* **535**, 266–270 (2016).
38. K. D. Usadel, Generalized diffusion equation for superconducting alloys. *Phys. Rev. Lett.* **25**, 507–509 (1970).
39. C. Shekhar, A. K. Nayak, Y. Sun, M. Schmidt, M. Nicklas, I. Leermakers, U. Zeitler, Y. Skourski, J. Wosnitza, Z. Liu, Y. Chen, W. Schnelle, H. Borrmann, Y. Grin, C. Felser, B. Yan, Extremely large magnetoresistance and ultrahigh mobility in the topological Weyl semimetal candidate NbP. *Nat. Phys.* **11**, 645–649 (2015).
40. N. De Leo, M. Fretto, V. Lacquaniti, C. Cassiago, L. D'Ortenzi, L. Boarino, S. Maggi, Thickness modulated niobium nanoconstrictions by focused ion beam and anodization. *IEEE Trans. Appl. Supercond.* **26**, 7100305 (2016).
41. D. Shoenberg, *Magnetic Oscillations in Metals* (Cambridge Univ. Press, 1984).


**Acknowledgments:** We thank A. Potter, A. Mackenzie, and M. Baenitz for stimulating discussions. **Funding:** Work by N.N. and J.G.A. is partly supported by the Office of Naval Research under the Electrical Sensors and Network Research Division, Award No. N00014-15-1-2674, and by the Gordon and Betty Moore Foundation's EPiQS Initiative through Grant GBMF4374. M.D.B. and P.J.W.M. acknowledge funding through the Max Planck Society. M.D.B. acknowledges studentship funding from EPSRC under grant no. EP/I007002/1. N.N. is supported by the NSF Graduate Research Fellowship Program under grant no. DGE 1106400. F.F. acknowledges support from a Lindemann Trust Fellowship of the English Speaking Union. R.I. is funded by the Air Force Office of Scientific Research Multidisciplinary University Research Initiative. T.M. is funded by Deutsche Forschungsgemeinschaft through GRK 1621 and SFB 1143. N.J.G. and E.D.B. were supported under the auspices of the U.S. Department of Energy, Office of Science. F.R. was supported by the Los Alamos National Laboratory Laboratory Directed Research and Development program. **Author contributions:** P.J.W.M. and J.G.A. designed the experiment. M.D.B. and N.N. fabricated the microstructures and performed the transport experiments. F.F., R.I., and T.M. contributed to the theory and models of proximity effect–induced superconductivity in WSMs. N.J.G., E.D.B., F.R., N.N., and J.G.A. grew and characterized the crystals. All authors were involved in writing the manuscript. **Competing interests:** The authors declare that they have no competing interests. **Data and materials availability:** All data needed to evaluate the conclusions in the paper are present in the paper. Additional data related to this paper may be requested from the authors. Data underpinning this publication can be accessed at http://dx.doi.org/10.17630/04280577-35c4-44e7-97d2-5c827ace7a4e.

Submitted 28 November 2016
Accepted 22 March 2017
Published 24 May 2017
10.1126/sciadv.1602983

**Citation:** M. D. Bachmann, N. Nair, F. Flicker, R. Ilan, T. Meng, N. J. Ghimire, E. D. Bauer, F. Ronning, J. G. Analytis, P. J. W. Moll, Inducing superconductivity in Weyl semimetal microstructures by selective ion sputtering. *Sci. Adv.* **3**, e1602983 (2017).

# Inducing superconductivity in Weyl semimetal microstructures by selective ion sputtering

Maja D. Bachmann, Nityan Nair, Felix Flicker, Roni Ilan, Tobias Meng, Nirmal J. Ghimire, Eric D. Bauer, Filip Ronning, James G. Analytis and Philip J. W. Moll

*Sci Adv* **3** (5), e1602983.
DOI: 10.1126/sciadv.1602983